Electronic Supplementary Material (ESI) for New Journal of Chemistry.

Systematic regulation of ligands realizes the transition of cuprous iodide inorganic-organic hybrid materials from blue to green light

Juan-Juan Shao, Jian-Ling Ni, Wei-Min Chen, Peng-Lai Liu, Abraham Mensah, Li-Zhuang Chen, and Fang-Ming Wang

[a] School of Environmental and Chemical Engineering, Jiangsu University of Science and Technology, Zhenjiang 212003, Jiangsu, P. R. China.

Supporting Information

Exprimental Section

Powder X-ray diffraction (PXRD) analysis.

Powder X-ray diffraction (PXRD) patterns were measured on Ultima IV with CuKα radiation field emission (λ=1.5406Å). Measurements were made in a 2ϑ range of 5−50°. The data were collected at room temperature with a scanning speed of 10°/min. The operating power was 40 kV/10 mA.

Photoluminescence spectra measurements and lifetime measurements.

Photoluminescence measurements of the complexes in the solid state were recorded using a FS5 fluorescence spectrophotometer at room temperature. The obtained sample powder was put into between two glass plates (which do not have emission in the visible range) for measurements. The lifetime decay data is also recorded a FS5 fluorescence spectrophotometer at room temperature. The lifetimes of the sample were extracted by fitting the decay curves in Origin with first, second or third order exponential decay functions with coefficient of determination (R^2) values larger than 0.99.

Thermogravimetric Analysis (TGA).

TG analyses were performed on powder samples by a Netzsch/TG209 F3 thermogravimeter. Pure powder samples were put into platinum pans and heated it from room temperature to 800°C at a heating rate of 10°C/min.

Optical Diffuse Reflectance Measurements.

Optical diffuse reflectance spectra were measured by a Shimadzu UV-3600 spectrophotometer with $BaSO_4$ powder as the standard (100% reflectance) at room temperature. The data were collected in the wavelength range of 300-800nm. In order to evaluate the band gap, the Kubelka-Munk function is used to collect and transform the data. The function conversion procedure is the same as reported in the past literature. The scattering coefficient (S) is considered to be a constant, because the average particle size of the measured sample is obviously greater than 5 μm.

Internal Quantum Yield Measurements

The room temperature internal quantum yields (IQYs) of samples in powder were measured on a C9920-03 absolute quantum yield measurement system (Hamamatsu Photonics) with 150 W xenon monochromatic light source and 3.3 inch integrating sphere. The sample to be measured is prepared by spreading the powder sample evenly on the bottom of the quartz sample holder.

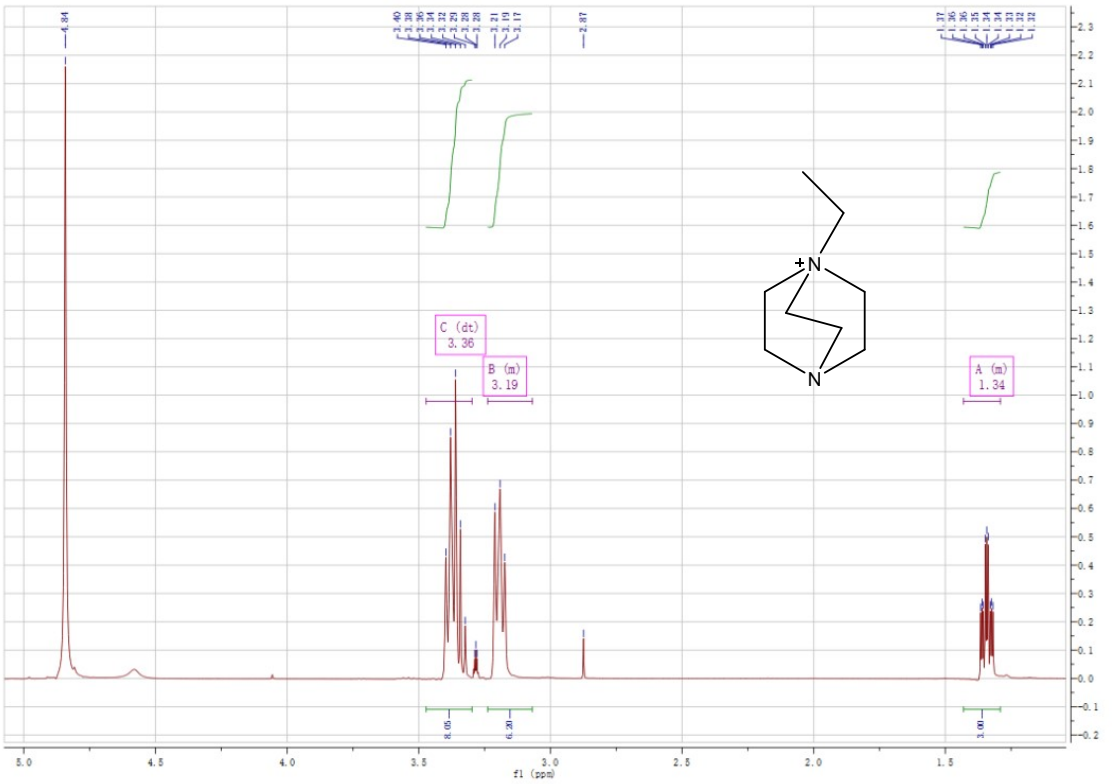

Fig.S1 H NMR spectrum of organic ligand $\mathbf{L_1}$

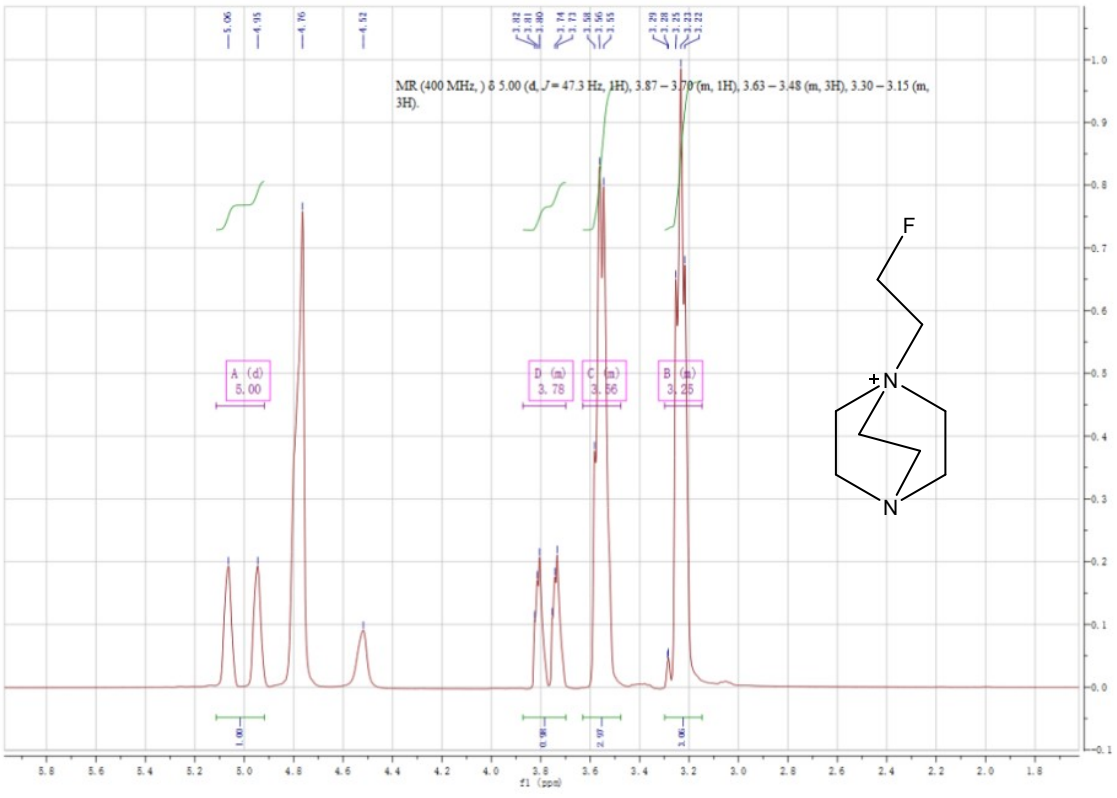

Fig.S2 H NMR spectrum of organic ligand $\mathbf{L_2}$

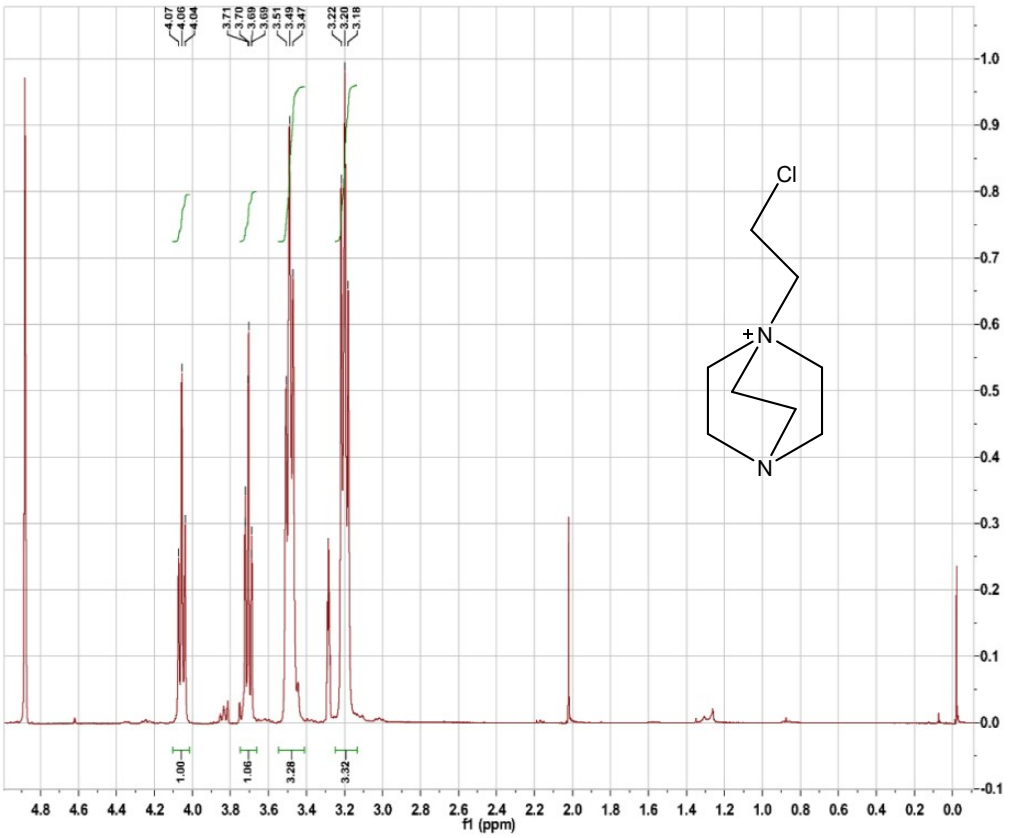

Fig.S3 H NMR spectrum of organic ligand $\mathbf{L_3}$

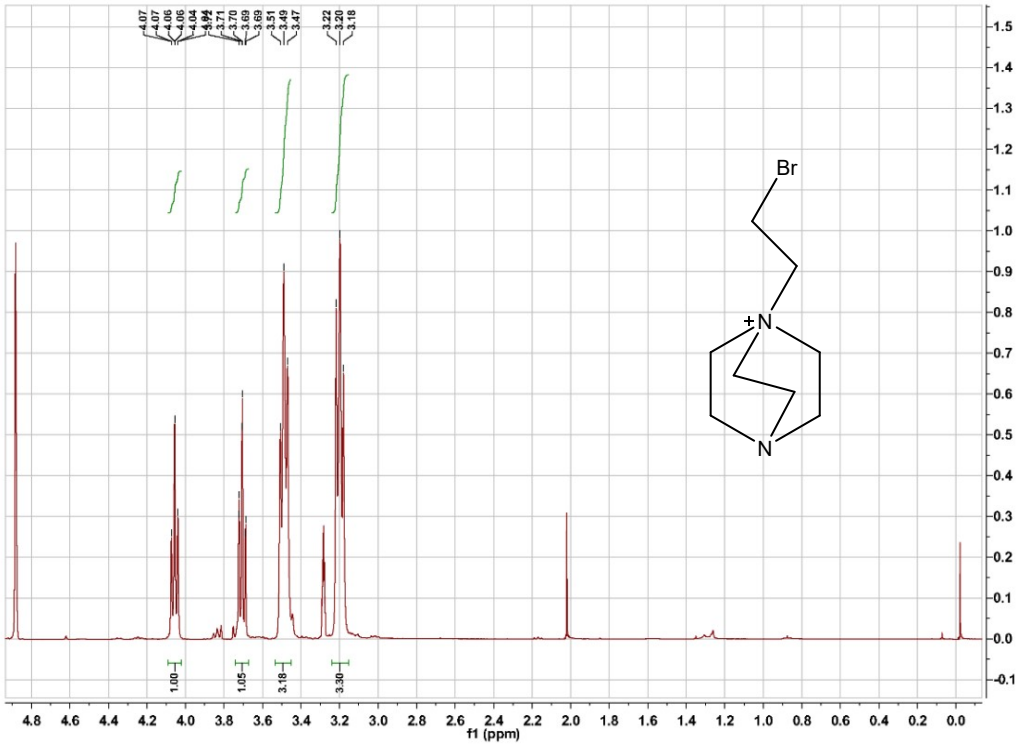

Fig.S4 H NMR spectrum of organic ligand $\mathbf{L_4}$

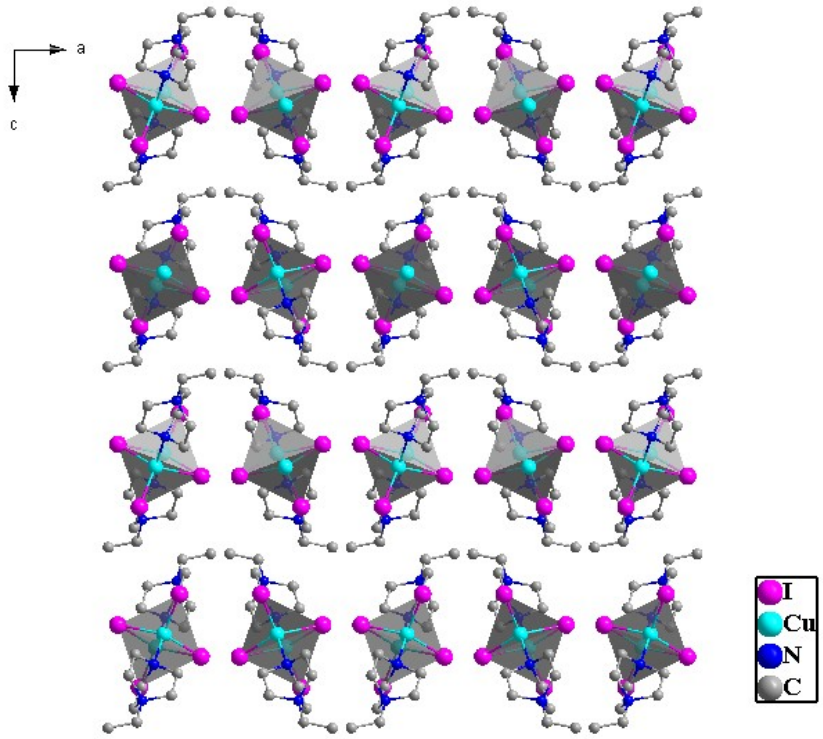

Fig.S5 Supramolecular network viewed along the *b*-axis of complex **1**

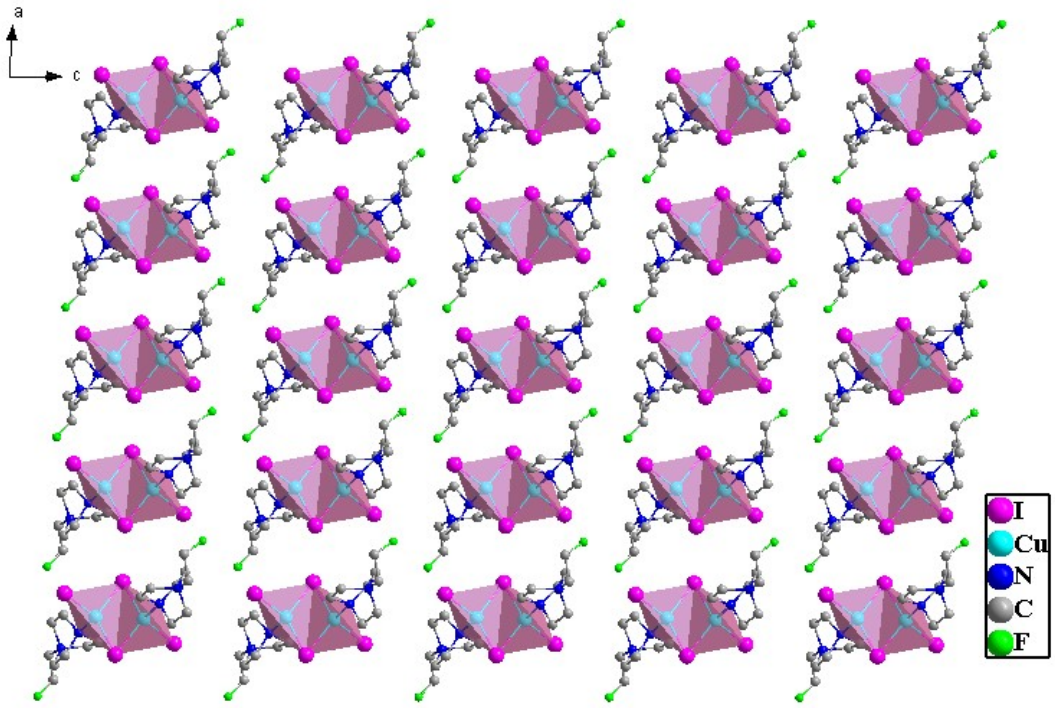

Fig.S6 Supramolecular network of complex **2**

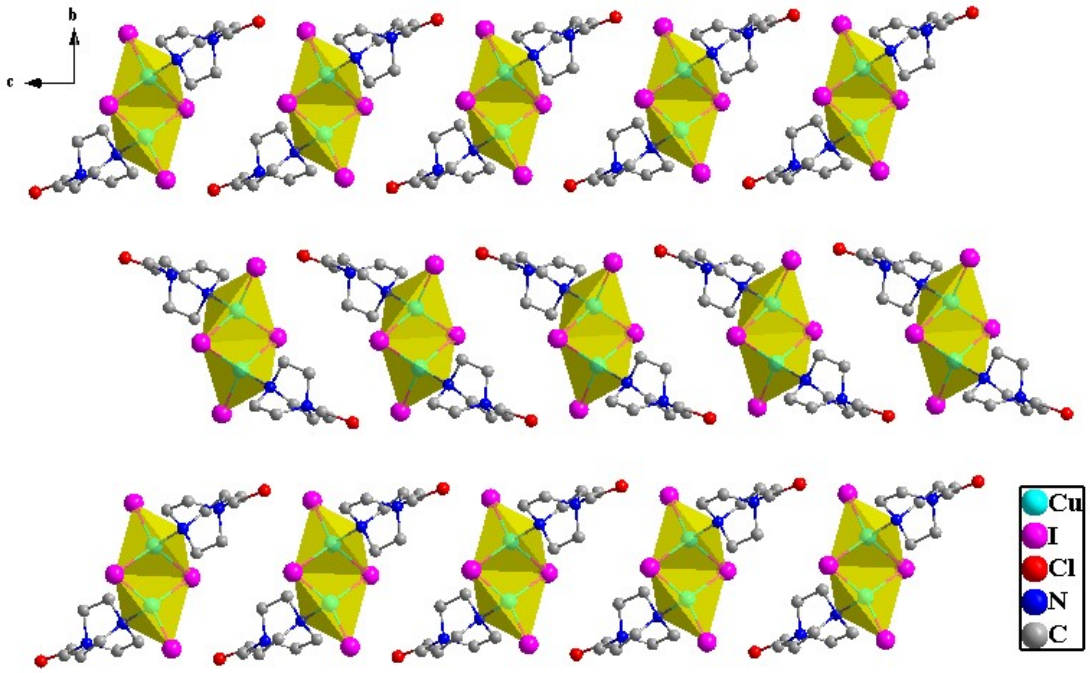

Fig.S7 Supramolecular network viewed along the *a*-axis of complex **3**

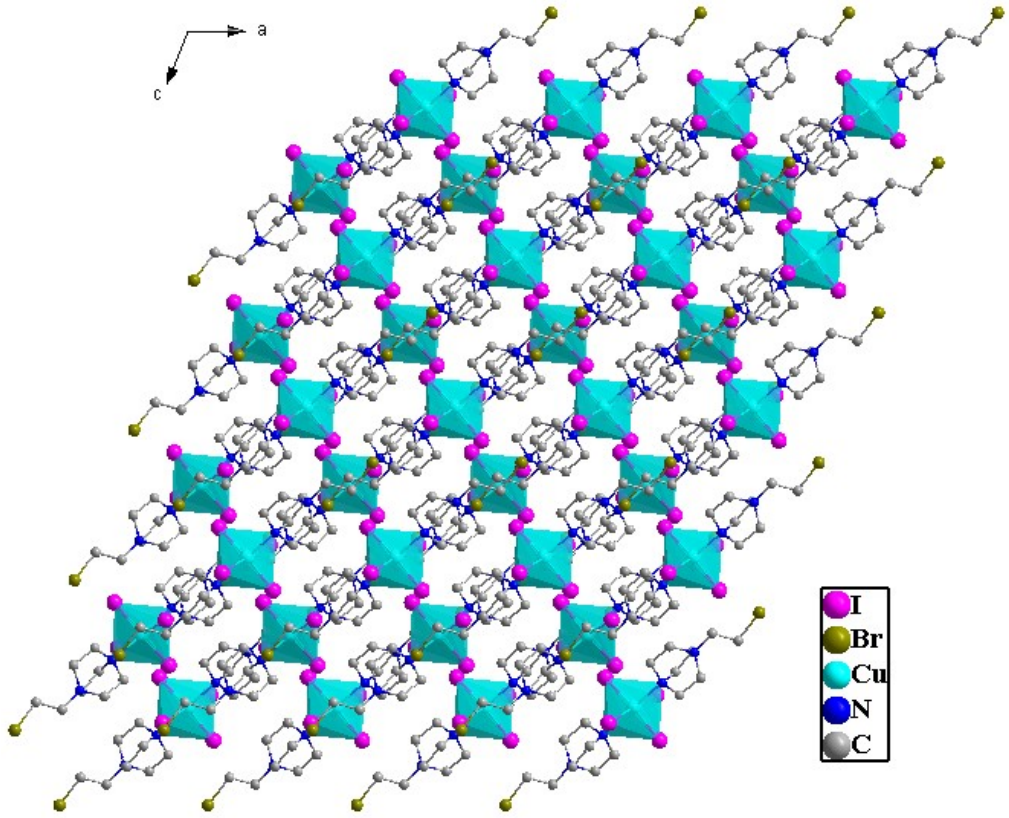

Fig.S8 Supramolecular network viewed along the b-axis of complex **4**

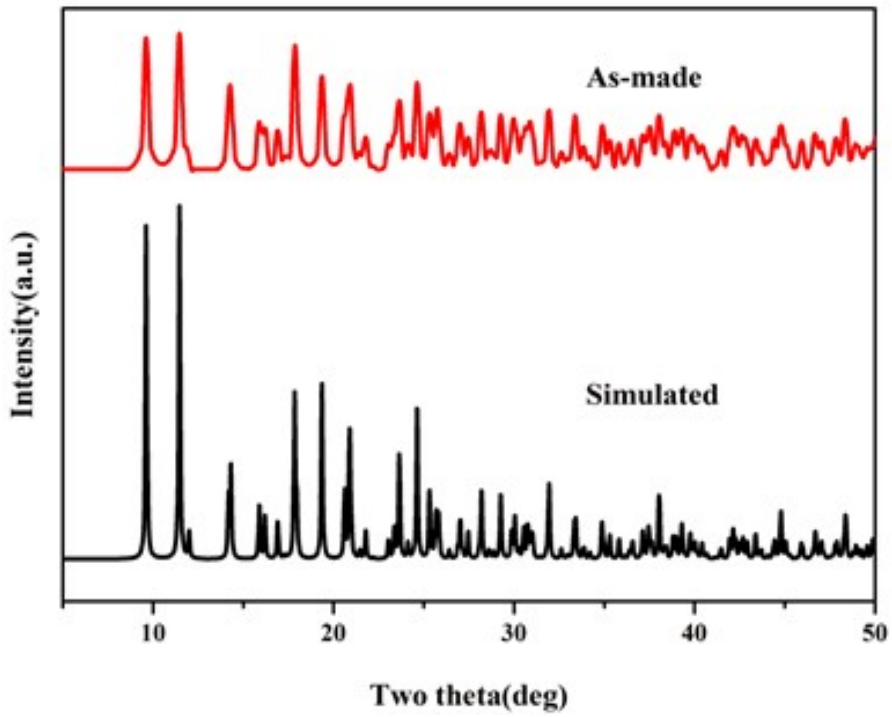

Fig.S9PXRD patterns of Complex **1**

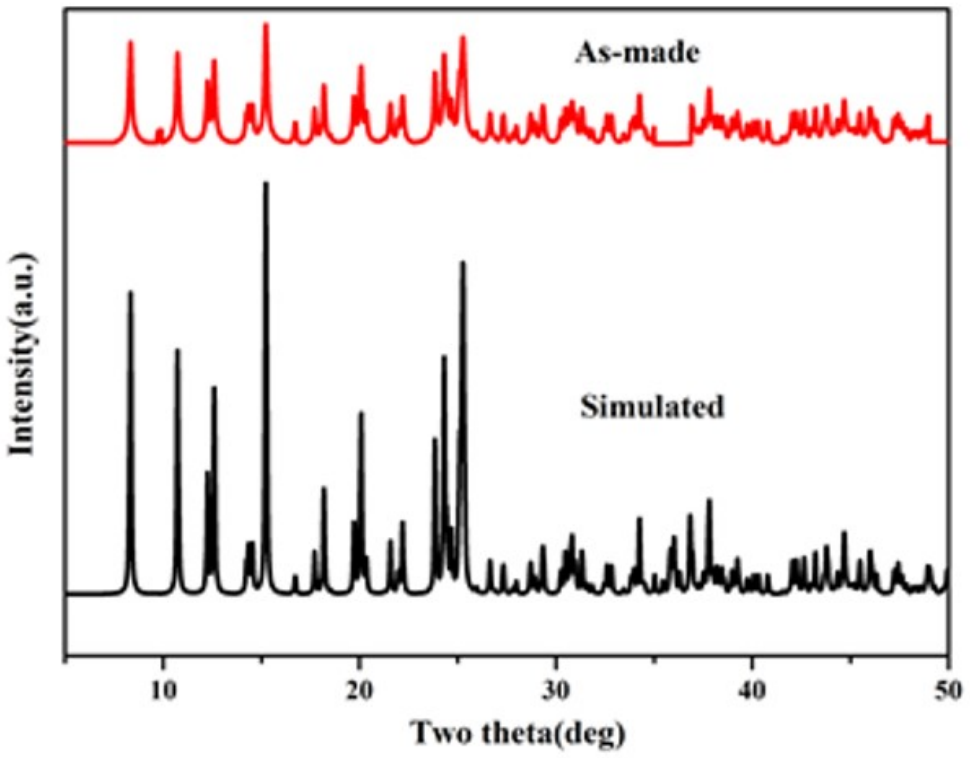

Fig.S10 PXRD patterns of Complex **2**

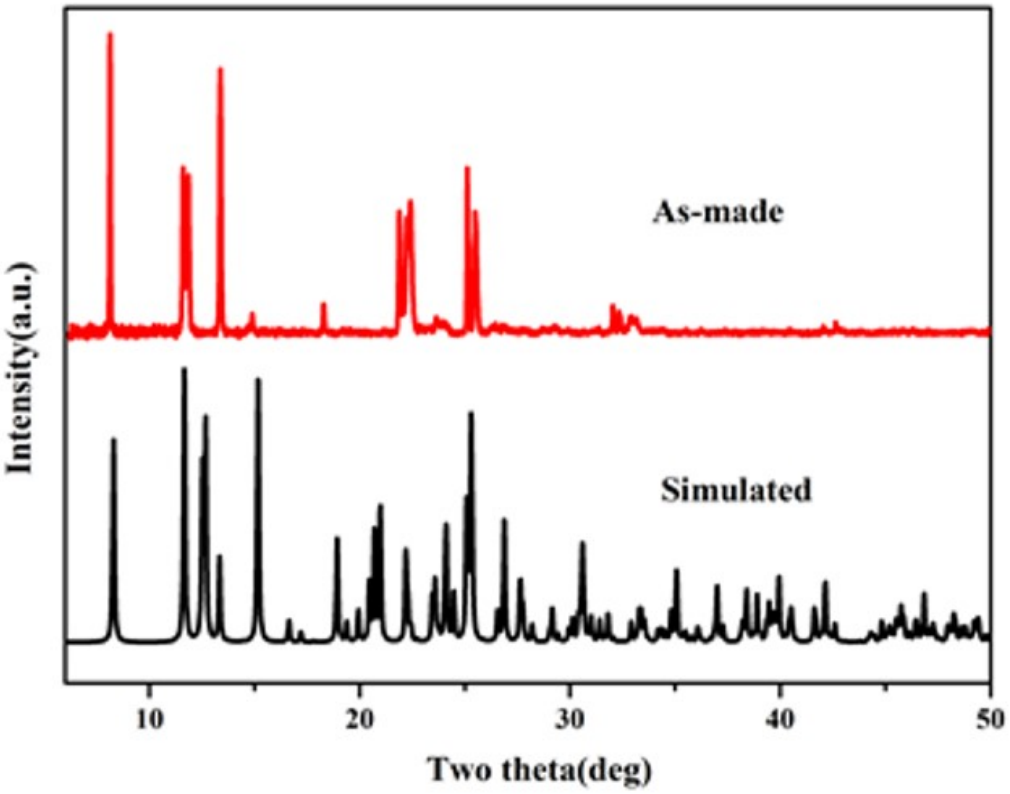

Fig.S11 PXRD patterns of Complex **3**

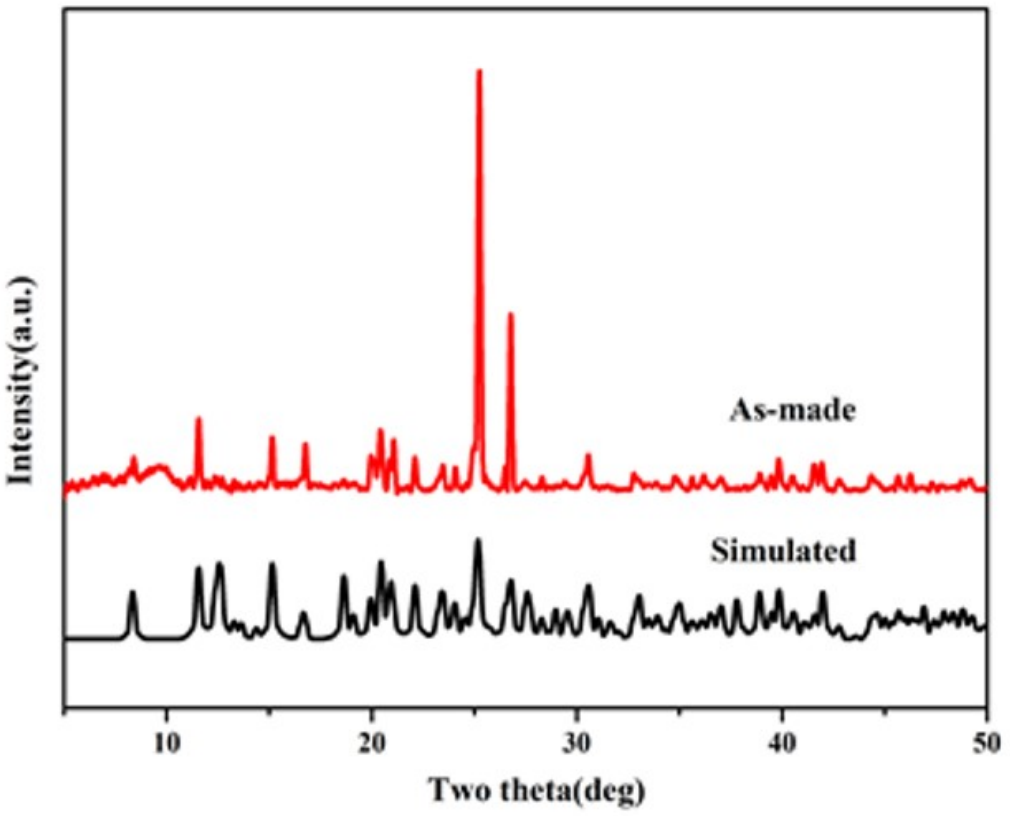

Fig.S12 PXRD patterns of Complex **4**

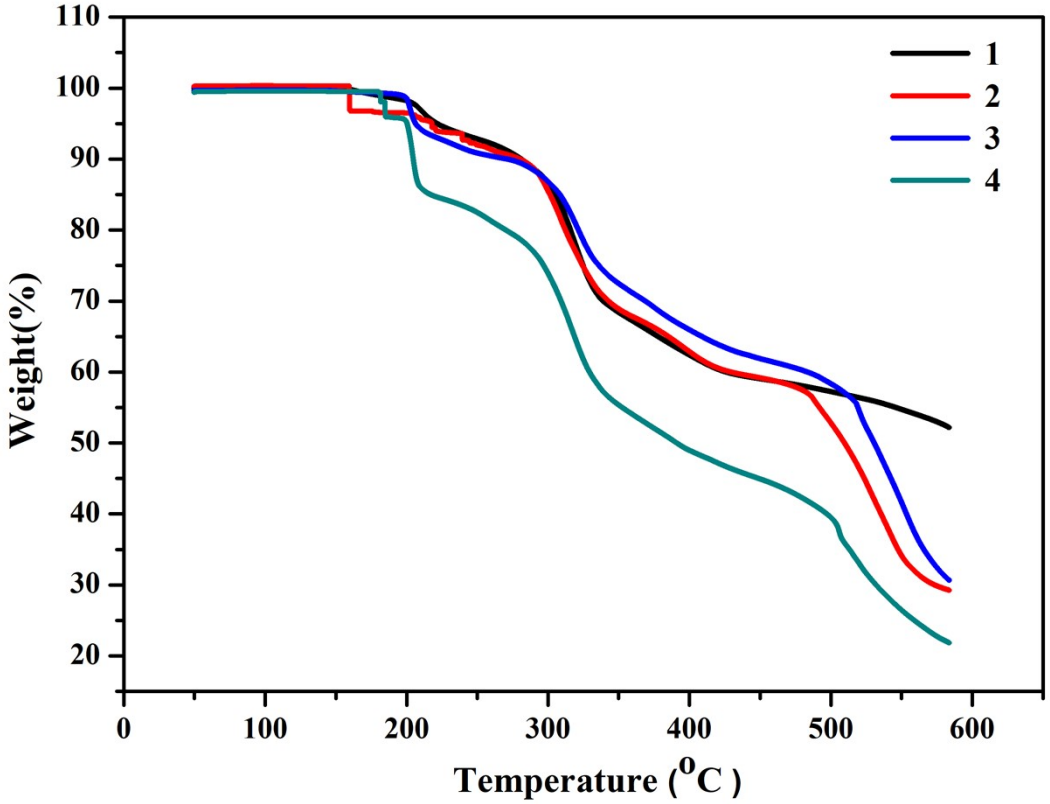

Fig. S13 TG curves of complexs **1-4**

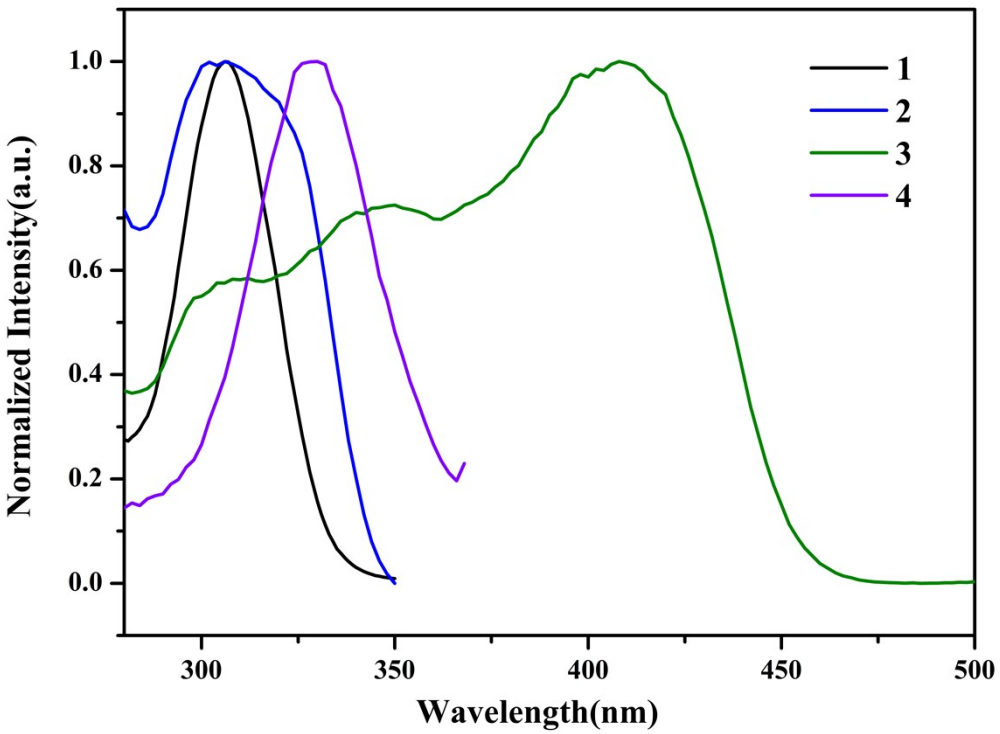

Fig.14 Excitation spectra of complexes **1-4**

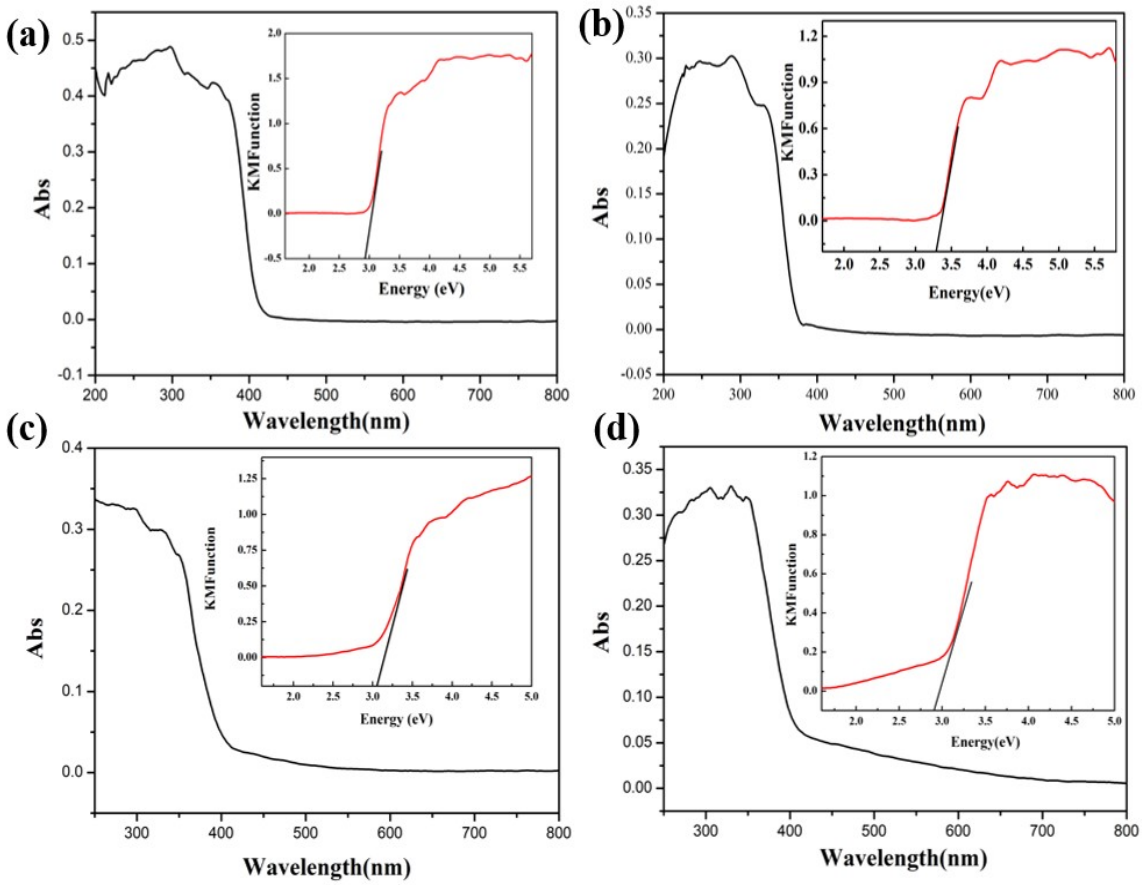

Fig.15 UV-vis absportion plots of complexs **1** (a), **2** (b), **3**(c) and **4**(d)

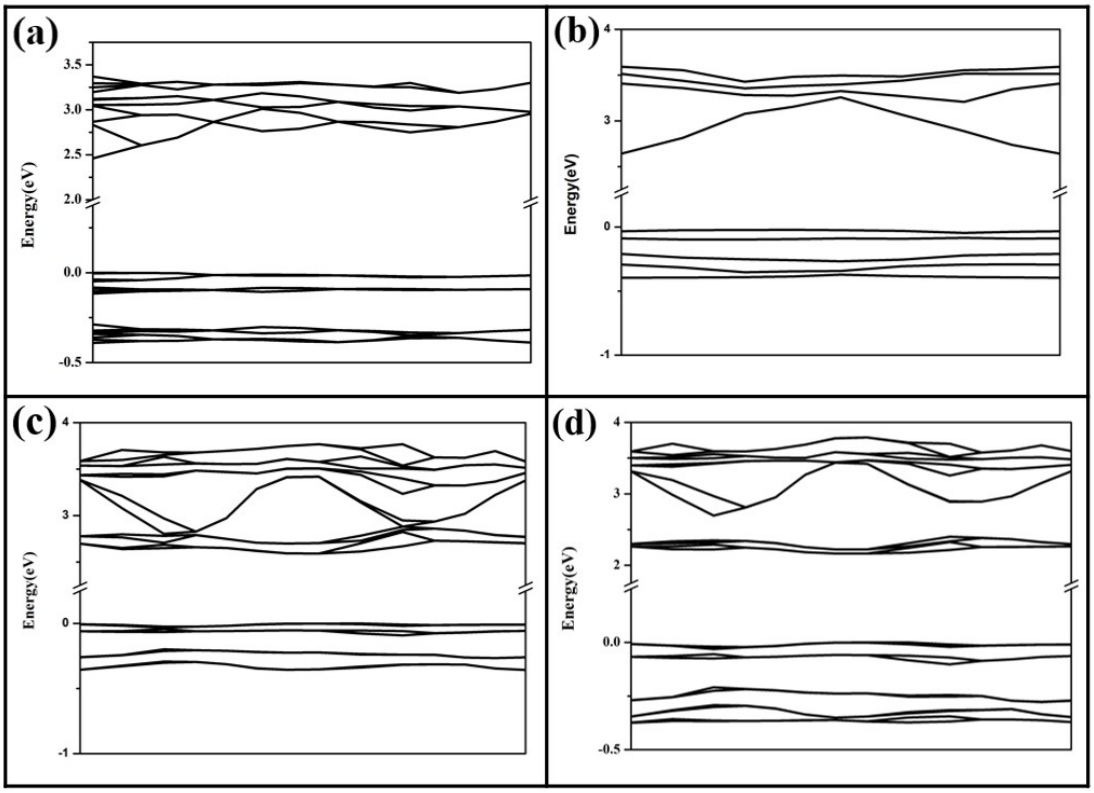

Fig.S16 Band gap of **1** (a) , **2** (b), **3**(c) and **4**(d)

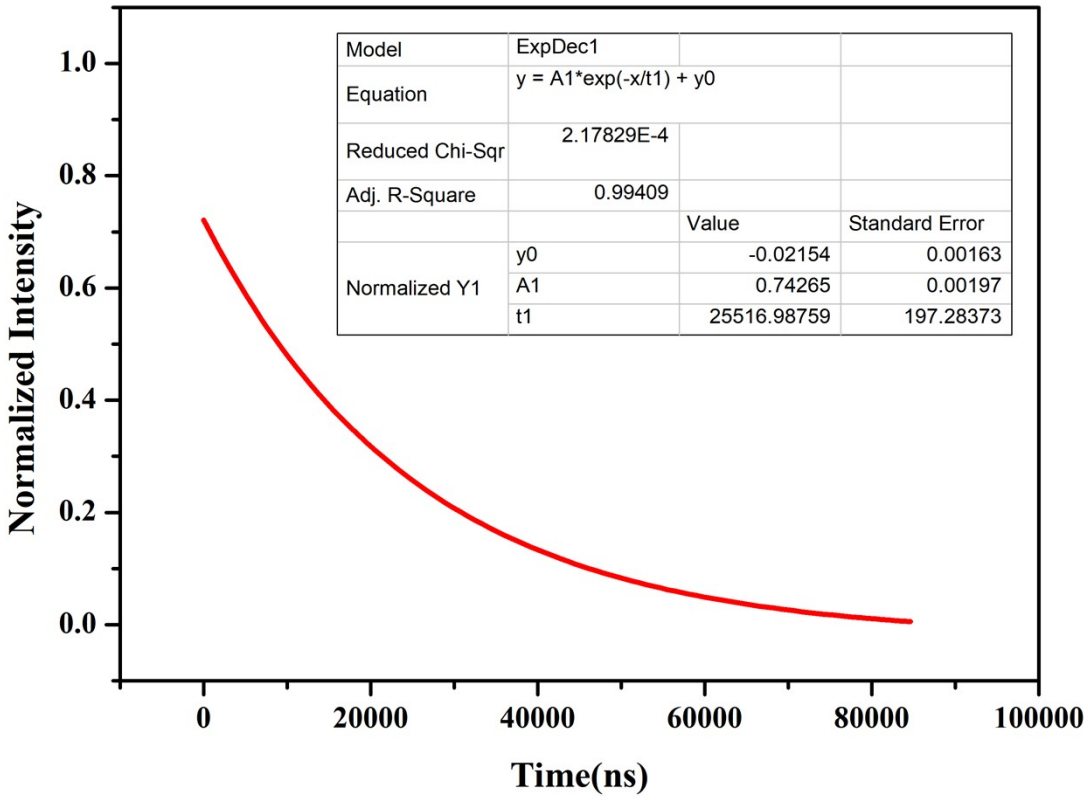

Fig.S17 Luminescent decay curve of complex **1**

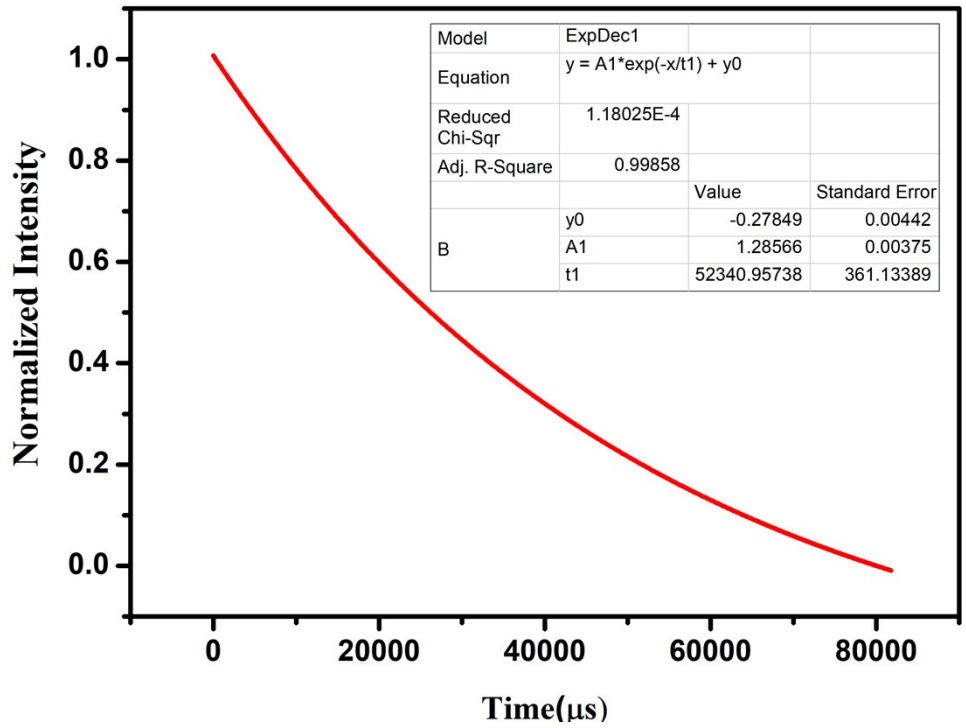

Fig.S18 Luminescent decay curve of complex **2**

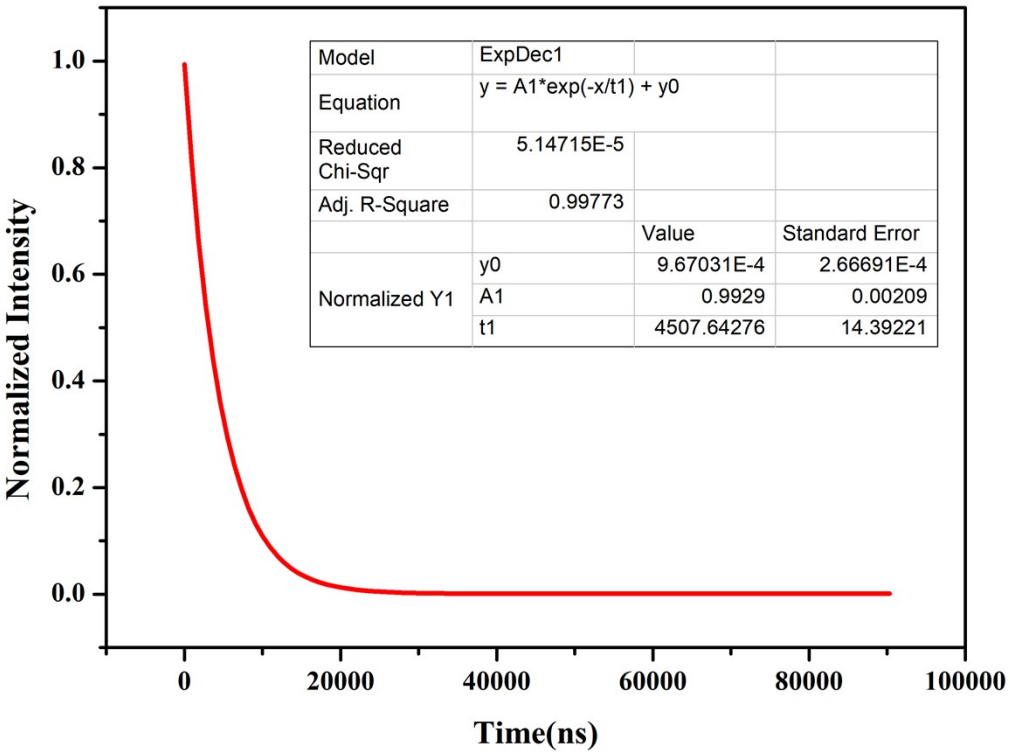

Fig.S19 Luminescent decay curve of complex **3**

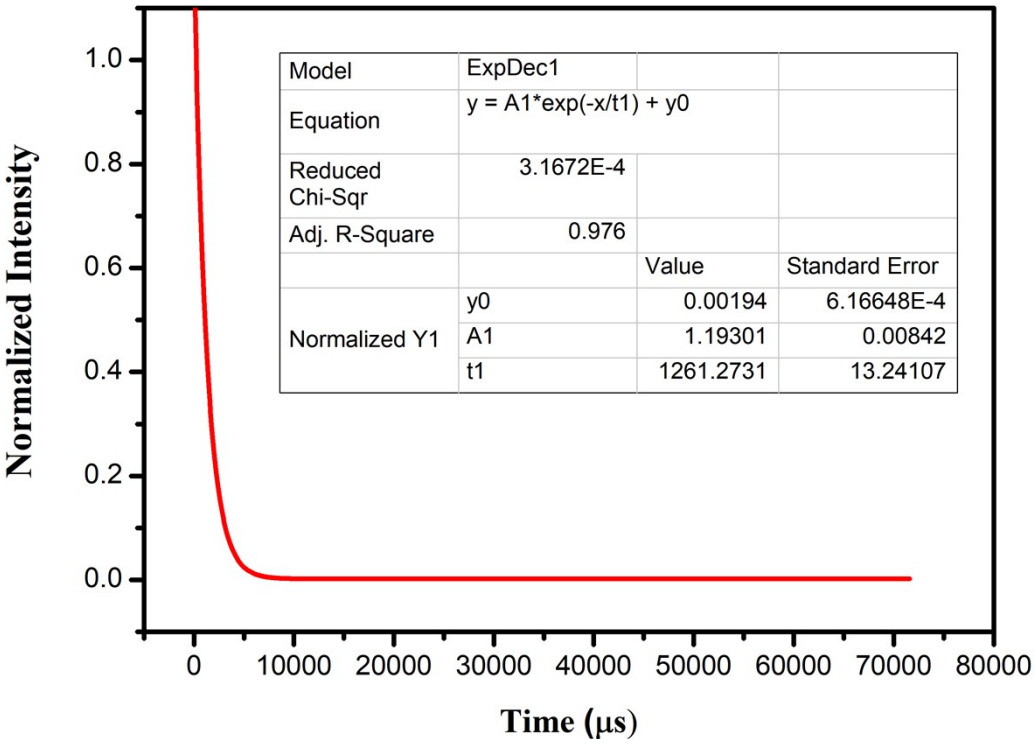

Fig.S20 Luminescent decay curve of complex **4**

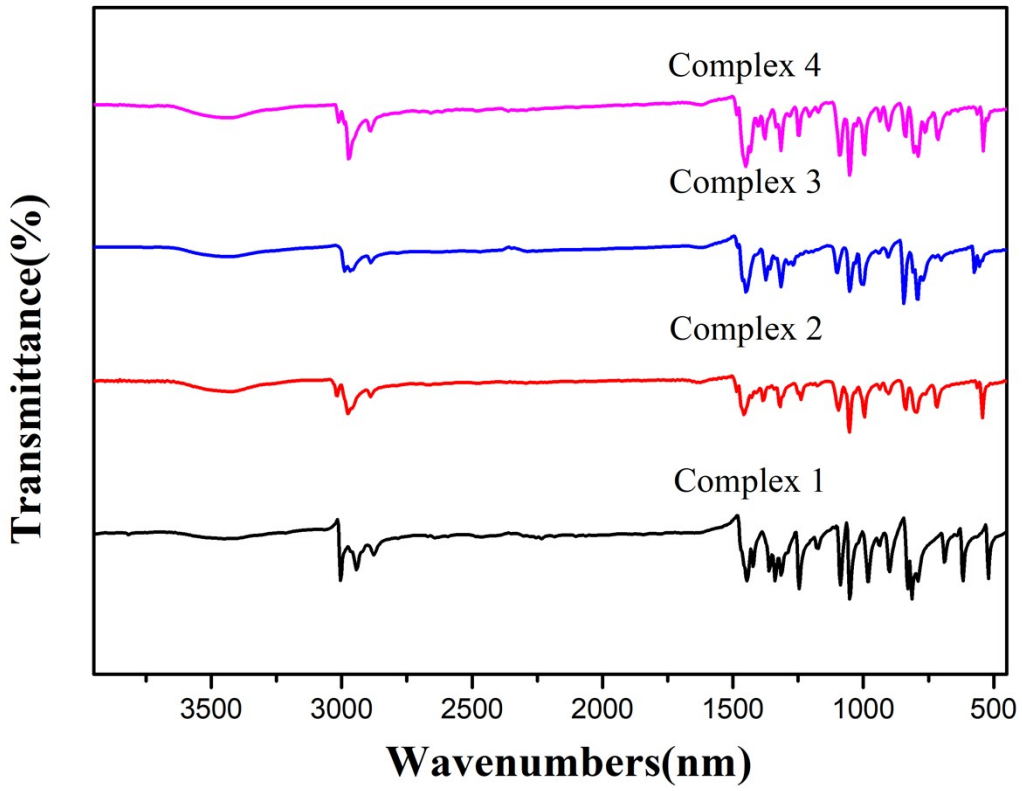

Fig.S21 FT-IR patterns of Complexs **1-4**

Table S1 Selected bond lengths (Å) and bond angles (°) of **1**

Bond	Dist.	Bond	Dist.	Bond	Dist.
I1-Cu1	2.6136(5)	I2-Cu1^{1}	2.6455(5)	I2-Cu1	2.6471(5)
Cu1-Cu1^{1}	2.7293(9)	Cu1-N1	2.183(3)	N1-C5	1.472(4)
Angle	(°)	Angle	(°)	Angle	(°)
Cu1^{1}-I2-Cu1	62.085(18)	I1-Cu1-I2^{1}	114.496(18)	I1-Cu1-I2	111.905(18)
I1-Cu1-Cu1^{1}	139.80(3)	I2^{1}-Cu1-I2	117.916(18)	I2-Cu1- Cu1^{1}	58.929(17)

Table S2 Selected bond lengths (Å) and bond angles (°) of **2**

Bond	Dist.	Bond	Dist.	Bond	Dist.
I1-Cu1	2.762(3)	I1-Cu2	2.621(3)	I3-Cu1	2.607(3)
I3-Cu2	2.724(3)	I2-Cu2	2.596(3)	I4-Cu1	2.583(3)
Cu1-Cu2	2.6685(10)	Cu1-N3	2.165(17)	Cu2-N1	2.179(17)
Angle	(°)	Angle	(°)	Angle	(°)
Cu2-I1-Cu1	59.37(7)	Cu1-I3-Cu2	60.03(7)	I3-Cu1-I1	119.84(11)
I3-Cu1-Cu2	62.16(7)	I4-Cu1-I1	103.56(10)	I4-Cu1-I3	118.67(12)

Table S3 Selected bond lengths (Å) and bond angles (°) of **3**

Bond	Dist.	Bond	Dist.	Bond	Dist.
Cu1 -Cu1^{1}	2.707(3)	Cu1-I1^{1}	2.6822(14)	Cu1-I1	2.6301(13)
Cu1-I2	2.5900(13)	Cu1-N1	2.182(6)	Cl1-C8	1.849(9)
Angle	(°)	Angle	(°)	Angle	(°)
I1-Cu1- I1^{1}	118.74(5)	I2-Cu1-I1^{1}	107.97(5)	I2-Cu1- Cu1^{1}	101.41(18)
Cu1-I1 -Cu1^{1}	61.26(5)	I2-Cu1-I1	115.56(5)	Cu1^{1}- Cu1-I1^{1}	107.97(5)

Table S4 Selected bond lengths (Å) and bond angles (°) of **4**

Bond	Dist.	Bond	Dist.	Bond	Dist.
I1-Cu1	2.5894(8)	I2-Cu1	2.6275(8)	I2-Cu1^{1}	2.6739(9)
Cu1-Cu1^{1}	2.7282(15)	Cu1-N1	2.181(4)	N1-C1	1.465(7)
Angle	(°)	Angle	(°)	Angle	(°)
Cu1-I2-Cu1^{1}	61.94(3)	I1-Cu1-I2^{1}	108.69(3)	I1-Cu1-I2	115.76(3)
I1-Cu1-Cu1^{1}	137.10(4)	I2-Cu1-I2^{1}	118.06(3)	I2-Cu1-Cu1^{1}	59.87(3)